Generation of Pure-State Single-Photon Wavepackets by Conditional Preparation Based on Spontaneous Parametric Downconversion

A. B. U'Ren[1, 2], C. Silberhorn[1], K. Banaszek[1], I. A. Walmsley[1], *, R. Erdmann[3], W. P. Grice[4], and M. G. Raymer[5]

[1] *Clarendon Laboratory, Oxford University, Oxford, OX1 3PU, UK*

[2] *Department of Optics, Centro de Investigación Científica y Educación Superior de Ensenada (CICESE), Baja California, 22860 Mexico*

[3] *Rome Air Force Laboratory, Rome, NY, USA*

[4] *Center for Engineering Science Advanced Research, Computer Science and Mathematics Division, Oak Ridge National Laboratory, Oak Ridge, Tennessee 37831, USA*

[5] *Department of Physics and Oregon Center for Optics, University of Oregon, Oregon 97403, USA*

*e-mail: walmsley@physics.ox.ac.uk
Received September 17, 2004

Abstract—We study the conditional preparation of single photons based on parametric downconversion, where the detection of one photon from a given pair heralds the existence of a single photon in the conjugate mode. We derive conditions on the modal characteristics of the photon pairs, which ensure that the conditionally prepared single photons are quantum-mechanically pure. We propose specific experimental techniques that yield photon pairs ideally suited for single-photon conditional preparation.

1. INTRODUCTION

Pure single-photon states are probably the most fundamental entities in quantum optics and constitute the starting point for many optically based quantum-enhanced technologies. A basic requirement for many key applications is the ability to generate reliably pure single-photon wavepackets capable of high-visibility interference. Single-photon wavepackets may be generated from number-correlated pairs by conditional state preparation. For example, photon pairs produced by the process of spontaneous parametric downconversion (PDC) in a $\chi^{(2)}$ nonlinear medium allow for the conditional preparation of single photons, since the detection of one photon in the pair heralds the presence of the conjugate photon. PDC-generated photons have been employed for both fundamental tests of quantum mechanics and to demonstrate various quantum-communication applications, such as quantum teleportation [1], quantum dense coding [2], and quantum cryptography [3].

A recent proposal for linear optical quantum computation (LOQC) [4] exploits the photon bunching that occurs in quantum interference between pure-state single photons in conjunction with conditional state preparation in linear optical networks. In the latter, detection of auxiliary photons indicates the successful operation of a given gate. For LOQC, as for all other applications involving optical quantum networks, high-visibility interference between photons from multiple sources is crucial. This necessitates, on the one hand, precise timing of the photons used which, in turn,

demands a high probability of simultaneous generation from synchronized distinct sources. On the other hand, precise control of the modal structure of the generated photon pairs is essential in order to guarantee the purity of the conditionally prepared photon states. For independent sources, the interference of two single-photon wavepackets results in photon bunching only if the paths of the photons are indistinguishable. In other words, distinguishing information about the incoming photons, which always exists for mixed-state wavepackets, hinders the two-photon interference of independently generated single-photon wavepackets. For PDC-based implementations, these requirements lead to the need for a pulsed pump and for efficient sources exhibiting high brightness and detection efficiencies. Spatial modal control of the emitted photons and a much-increased production rate of photon pairs may result from waveguided PDC [5].

A common approach to guaranteeing indistinguishability in optical experiments uses strong spatial and spectral filtering. The cost of this, however, is a prohibitive reduction of the generation rate of usable single-photon wavepackets. Since birefringent phase matching leads to spatial–spectral correlations with overlapping contributions, spatial filtering also causes optical losses for the signal photon for finite spectral filter bandwidths. As a consequence, a photon is not always present in the signal arm when the trigger arm sounds a herald. In such a situation, one cannot rely with certainty on the single-photon preparation, because the signal arm may contain a vacuum state. The fidelity,

which measures the probability of finding a one-photon state in the signal arm, is limited by vacuum contributions. To eliminate these and to ensure, for example, successful gate operations in LOQC, postselection by coincidence measurements is inevitable. But such postselection, in turn, hinders the realization of scalable networks involving more than one or possibly two sources. Waveguided PDC is one route to accomplishing both the decorrelation of the spatial degrees of freedom from spectral ones and the elimination of the signal–idler spatial correlations. Thus, the need for spatial filtering is eliminated; however, conditionally prepared single photons are unfortunately in general still described by a mixed state due to spectral correlations present in the photon pairs. In this paper, we study the conditional state preparation of single-photon wavepackets based on PDC pumped by ultrafast pulses. We use a multimode description and propose novel engineering techniques for preventing correlations involving unobserved variables. This ensures that the detection of one photon from a given pair directly yields a pure-state single-photon wavepacket in the conjugate mode, without resorting to filtering. The development of bright pure single-photon sources constitutes an important step in the further development of quantum networks, permitting high-visibility interference between independently generated photons and a high simultaneous coincidence detection rate from multiple sources.

2. CONDITIONAL STATE PREPARATION OF PURE-STATE SINGLE-PHOTON WAVEPACKETS IN A MULTIMODE DESCRIPTION

Single-photon states are defined as containing a single quantum in the photon-number basis. A complete specification of the photons requires that all degrees of freedom associated with the quantized electromagnetic field of the occupied optical modes be taken into account. Thus, the complete description of the photons involves the polarization, the spatial vector $\mathbf{r}$ or wavevector $\mathbf{k}$, and the frequency ω or time dependence t of the underlying quantum field. The dispersion relationship between $\mathbf{k}$ and ω reduces one degree of freedom, so that we can restrict our analysis to transverse wavevectors $\mathbf{k}^\perp$. For simplicity, we also consider only a single polarization, which is appropriate for PDC experiments aimed at the conditional preparation of single photons. A pure-state single-photon wavepacket can then be defined as a coherent superposition of monochromatic plane waves [7]:

$$|\phi\rangle = N \int d\omega \int d\mathbf{k}^\perp c(\omega, \mathbf{k}^\perp)$$
$$\times \exp[i(\mathbf{k}^\perp \cdot \mathbf{r} - \omega t)]\hat{a}^\dagger(\omega, \mathbf{k}^\perp)|0\rangle, \quad (1)$$

where N denotes the normalization constant and the coefficient function $c(\omega, \mathbf{k}^\perp)$ determines the modal structure of the photon. The corresponding density operator is given by $\rho = |\phi\rangle\langle\phi|$ and exhibits nonzero off-diagonal elements. This is to be contrasted with a completely mixed single-photon wavepacket in frequency and momentum, for which no coherence between the different modes exists and which is characterized by a density operator of the form [8]

$$\hat{\rho} = N \int d\omega \int d\mathbf{k}^\perp |c(\omega, \mathbf{k}^\perp)|^2 \hat{a}^\dagger(\omega, \mathbf{k}^\perp)|0\rangle\langle 0|\hat{a}(\omega, \mathbf{k}^\perp), \quad (2)$$

which does not exhibit any off-diagonal elements.

In the process of PDC, individual pump photons split into two daughter photons in modes $\hat{a}$ and $\hat{b}$. A perturbative analysis with the interaction Hamiltonian of the $\chi^{(2)}$ process for a strong pump field, which is treated classically, results in a state of the form

$$|\Psi\rangle = |0\rangle|0\rangle + \mu \int\int d\omega_s d\omega_i \int\int d\mathbf{k}_s^\perp d\mathbf{k}_i^\perp$$
$$\times F(\omega_s, \mathbf{k}_s^\perp; \omega_i, \mathbf{k}_i^\perp)\hat{a}^\dagger(\omega_s, \mathbf{k}_s^\perp)\hat{b}^\dagger(\omega_i, \mathbf{k}_i^\perp)|0\rangle, \quad (3)$$

where μ is a measure of the efficiency of the PDC process and the function $F(\omega_s, \mathbf{k}_s^\perp; \omega_i, \mathbf{k}_i^\perp)$ represents a weighting function for the different spatial and spectral modes that are present, which results from the pump envelope and phase-matching functions defined by the specific downconversion configuration [8]. For the purpose of conditional-state preparation, the modes a and b should be distinguishable in at least one degree of freedom, which can be polarization for collinear type-II phase matching or the direction of propagation for noncollinear (type-I or type-II) phase matching. It is assumed that the pump power is low enough that the PDC process is spontaneous, thus ensuring that higher-photon-number contributions can be ignored. The function $F(\omega_s, \mathbf{k}_s^\perp; \omega_i, \mathbf{k}_i^\perp)$ may contain correlations between the signal and idler photons in the spatiotemporal continuous degrees of freedom, thus yielding an entangled two-photon pair. A useful tool for analyzing such entanglement is a Schmidt decomposition [9] of the spatiotemporal state amplitude. The Schmidt decomposition entails expressing the two-photon state in terms of complete basis sets of the orthonormal states $A_n^\dagger|0\rangle$ and $B_n^\dagger|0\rangle$, such that

$$|\Psi\rangle = \sum_n \sqrt{\lambda_n}\hat{A}_n^\dagger\hat{B}_n^\dagger|0\rangle, \quad (4)$$

where $\sum_n \lambda_n = 1$ and where the values λ_n are known as the Schmidt coefficients. In this description, the effective signal and idler creation operators $\hat{A}_n^\dagger$ and $\hat{B}_n^\dagger$ are

given in terms of the Schmidt functions $\psi_n(\omega_s, \mathbf{k}_s^{\perp})$ and $\phi_n(\omega_i, \mathbf{k}_i^{\perp})$ as

$$\hat{A}_n^{\dagger} = \int d\mathbf{k}_s^{\perp} \int d\omega_s \psi_n(\omega_s, \mathbf{k}_s^{\perp}) \hat{a}^{\dagger}(\omega_s, \mathbf{k}_s^{\perp})|0\rangle \qquad (5)$$

and

$$\hat{B}_n^{\dagger} = \int d\mathbf{k}_i^{\perp} \int d\omega_i \phi_n(\omega_i, \mathbf{k}_i^{\perp}) \hat{b}^{\dagger}(\omega_i, \mathbf{k}_i^{\perp})|0\rangle, \qquad (6)$$

while the two-photon state amplitude $F(\mathbf{k}_s^{\perp}, \omega_s; \mathbf{k}_i^{\perp}, \omega_i)$ can be expressed as

$$F(\omega_s, \mathbf{k}_s^{\perp}; \omega_i, \mathbf{k}_i^{\perp})$$
$$= \sum_n \sqrt{\lambda_n} \psi_n(\omega_s, \mathbf{k}_s^{\perp}) \phi_n(\omega_i, \mathbf{k}_i^{\perp}), \qquad (7)$$

where $\omega_{s,i}$ and $\mathbf{k}_{s,i}^{\perp}$ represent the frequency and the transverse wavevector of the signal and idler photons. For the calculation of the Schmidt functions themselves, the first step is to determine the reduced density matrices of the two subsystems corresponding to the signal and idler photons, which are defined by

$$\rho_s(\omega_s, \mathbf{k_s}^{\perp}; \tilde{\omega}_s, \tilde{\mathbf{k}}_s^{\perp})$$
$$= \iint d\omega' d\mathbf{k}^{\perp'} F(\omega_s, \mathbf{k}_s^{\perp}, \omega', \mathbf{k}^{\perp'}) F^*(\tilde{\omega}_s, \tilde{\mathbf{k}}_s^{\perp}, \omega', \mathbf{k}^{\perp'}) \qquad (8)$$

and

$$\rho_i(\omega_i, \mathbf{k}_i^{\perp}; \tilde{\omega}_i, \tilde{\mathbf{k}}_i^{\perp})$$
$$= \iint d\omega' d\mathbf{k}^{\perp'} F(\omega', \mathbf{k}^{\perp'}, \omega_i, \mathbf{k}_i^{\perp}) F^*(\omega', \mathbf{k}^{\perp'}, \tilde{\omega}_i, \tilde{\mathbf{k}}_i^{\perp}), \qquad (9)$$

and, as a second step, to solve the following integral eigenvalue equations [9]:

$$\iint d\omega' d\mathbf{k}^{\perp'} \rho_s(\omega_s, \mathbf{k}_s^{\perp}, \omega', \mathbf{k}^{\perp'}) \psi_n(\omega', \mathbf{k}^{\perp'})$$
$$= \lambda_n \psi_n(\omega_s, \mathbf{k}_s^{\perp}), \qquad (10)$$

$$\iint d\omega' d\mathbf{k}^{\perp'} \rho_i(\omega_i, \mathbf{k}_i^{\perp}, \omega', \mathbf{k}^{\perp'}) \phi_n(\omega', \mathbf{k}^{\perp'})$$
$$= \lambda_n \phi_n(\omega_i, \mathbf{k}_i^{\perp}), \qquad (11)$$

thus yielding the Schmidt functions ψ_n and ϕ_n and the joint eigenvalues λ_n as the Schmidt coefficients. The Schmidt decomposition simplifies the quantum-state description by turning the original state, expressed as a quadruple integral over frequency and transverse momentum variables, into a discrete sum that typically contains only a limited number of terms. The Schmidt functions $\psi_n(\omega_s, \mathbf{k}_s^{\perp})$ and $\phi_n(\omega_i, \mathbf{k}_i^{\perp})$ can be thought of as the basic building blocks of entanglement in the sense that, if the signal photon is determined to be described by a function ψ_n, we know with certainty that its idler sibling is described by the corresponding func-

tion ϕ_n. The Schmidt modes also represent space–time localized wavepackets [6] and may be thought of as the wavefunctions of a photon [7]. The probability of extracting a specific pair of modes $[\psi_n(\omega_s, \mathbf{k}_s^{\perp}), \phi_n(\omega_i, \mathbf{k}_i^{\perp})]$ is given by the parameter λ_n, which is real and nonnegative. The amount of entanglement can be conveniently quantified by the cooperativity parameter [10], which is defined in terms of the Schmidt eigenvalues as

$$K = \frac{1}{\sum_n \lambda_n^2}. \qquad (12)$$

The value of K gives an indication of the number of active Schmidt mode pairs, which in turn is a measure of how much entanglement is present in the photon pairs. A two-photon state for which the cooperativity assumes its minimum allowed value $K = 1$ represents a state in which there is a single pair of active Schmidt mode functions, and which therefore exhibits no spectral or spatial entanglement. Another measure of the degree of nonseparability is the so-called entropy of entanglement:

$$S = -\sum_n \lambda_n \log(\lambda_n), \qquad (13)$$

which vanishes for a factorizable state and increases monotonically with the amount of entanglement present.

For the conditional state preparation of single-photon wavepackets via parametric downconversion, the idler photon is treated as a trigger, such that, in the ideal case of perfect photon number correlations, a detection event of the trigger idler channel heralds the emission of a photon in the signal channel. The quantum state resulting from this conditional preparation can be obtained by modeling the trigger detection process in terms of a projection operator and tracing over the trigger channel photon:

$$\hat{\rho}_s = \text{Tr}_i(\hat{\rho}\hat{\Pi}), \qquad (14)$$

where the subscript i denotes a partial trace acting over the trigger idler mode, $\hat{\rho}$ is the density operator describing the two-photon PDC state, and $\hat{\Pi}$ is the measurement operator modeling the trigger-photon detection. From the Schmidt decomposition, it can be easily seen that filtering one specific Schmidt mode $\phi_n(\omega_i, \mathbf{k}_i^{\perp})$ with the projection operator $\hat{B}_n^{\dagger}|0\rangle\langle0|\hat{B}_n$ allows for the conditional preparation of a pure photonic wavepacket in the signal mode. However, this procedure requires coherent frequency–time and spatial filters, which are nontrivial to implement.

We thus proceed to investigate the synthesis of pure signal photons by the time-integrated detection of the trigger idler photon in combination with passive spec-

tral and spatial (pinhole) filters. Correlations between the signal and idler photons generally lead to incoherence between different frequency and spatial components upon detection, yielding a mixed output-signal state. Physically, a measurement of the trigger reveals some information about the properties of the idler. A spatial and time-integrated detection of the idler state with a spectral interference filter and a spatial filter with a transfer functions $\sigma(\omega)$ and $\xi(\mathbf{k}^{\perp})$ respectively can be modeled by the projection operator

$$\hat{\Pi} = \int dt \int d\mathbf{r} \iint d\omega d\tilde{\omega} \iint d\mathbf{k} d\tilde{\mathbf{k}}^{\perp} \sigma(\omega) \xi(\mathbf{k}^{\perp})$$

$$\times \exp[i(\mathbf{k}\cdot\mathbf{r}-\omega t)]\hat{b}^{\dagger}(\omega,\mathbf{k})|0\rangle_i\langle 0|_i\hat{b}(\tilde{\omega},\tilde{\mathbf{k}})$$

$$\times \exp[-i(\tilde{\mathbf{k}}\cdot\tilde{\mathbf{r}}-\tilde{\omega}t)]\sigma^*(\tilde{\omega})\xi^*(\tilde{\mathbf{k}}^{\perp}) \quad (15)$$

$$= \int d\omega \int d\mathbf{k}^{\perp}|\sigma(\omega)|^2|\xi(\mathbf{k}^{\perp})|^2\hat{b}^{\dagger}(\omega,\mathbf{k})|0\rangle_i\langle 0|_i\hat{b}(\omega,\mathbf{k}).$$

By carrying out the calculation expressed by Eq. (14) using the density operator $|\Psi\rangle\langle\Psi|$ of the PDC state, it can be shown that the quantum state describing the signal channel, upon registering a trigger detection event, is given by

$$\hat{\rho}_s = \int d\omega \int d\mathbf{k}^{\perp} \int d\omega_s \int d\mathbf{k}_s^{\perp} \int d\tilde{\omega}_s \int d\tilde{\mathbf{k}}_s^{\perp}$$

$$\times |\sigma(\omega)|^2|\xi(\mathbf{k}^{\perp})|^2 F(\omega_s,\mathbf{k}_s^{\perp};\omega,\mathbf{k}^{\perp})\hat{a}^{\dagger}(\omega_s,\mathbf{k}_s^{\perp}) \quad (16)$$

$$\times |0\rangle_s\langle 0|_s\hat{a}(\tilde{\omega}_s,\tilde{\mathbf{k}}_s^{\perp})F^*(\tilde{\omega}_s,\tilde{\mathbf{k}}_s^{\perp};\omega,\mathbf{k}^{\perp}).$$

If we utilize the Schmidt decomposition of Eq. (7), the density operator of the conditionally prepared signal photon can be equivalently rewritten as

$$\hat{\rho}_s = \sum_n\sum_m \sqrt{\lambda_n\lambda_m}\int d\omega\int d\mathbf{k}^{\perp}|\sigma(\omega)|^2|\xi(\mathbf{k}^{\perp})|^2$$

$$\times \phi_n(\omega,\mathbf{k}^{\perp})\phi_m^*(\omega,\mathbf{k}^{\perp})\hat{A}_n^{\dagger}|0\rangle_s\langle 0|_s\hat{A}_m. \quad (17)$$

Under what conditions does $\hat{\rho}_s$ represent a pure state? Purity requires that the density operator $\hat{\rho}_s$ contains a single term, so that the signal state can be expressed in terms of a single Schmidt mode. From the expressions in Eqs. (16) and (17), two approaches to achieving purity for the conditional-state preparation via PDC become apparent. Restricting the trigger detection bandwidth to a single spectral component, i.e., $|\sigma(\omega)| \longrightarrow \delta(\omega-\Omega)$, as well as applying strong spatial filtering with imaging lenses and a narrow pinhole, i.e., $|\xi(\mathbf{k}^{\perp})| \longrightarrow \delta(\mathbf{k}^{\perp}-\mathbf{K})$, effectively suppresses the integration over ω and $\mathbf{k}^{\perp}$ in Eq. (16) and eliminates the incoherent sum over different frequency and spatial components, leaving the signal photon in a coherent superposition of monochromatic plane waves. Note, however, that this method for purifying the prepared signal-output state necessarily implies a sharp reduction of count rates and approaches truly pure states only

in the limit of vanishing counts. The Schmidt decompositions suggest an alternative route for the preparation of pure signal-photon states that exploits PDC pair generation. If the two-photon state is given in terms of a single Schmidt pair, the sums in Eq. (17) disappear, and the double integral term becomes an overall multiplicative constant. The latter implies that the prepared photon now forms a truly quantum-mechanically pure state. For a better understanding of this result, we can relate the Schmidt decomposition to the correlations between the generated photons. The excitation of only one Schmidt mode is actually equivalent to the statement that the PDC two-photon state is factorizable. Under such circumstances, the spectral and spatial properties of the signal and the idler photons are independent from each other, so that the detection of the idler photon yields no information whatsoever about the signal photon. In order to further quantify the purity of the conditionally prepared single photons in the signal arm, we can use the purity parameter p, which is defined as

$$p = \text{Tr}(\hat{\rho}_s^2). \quad (18)$$

Evaluating the purity p in terms of the Schmidt decomposition, we can clarify the connection between the purity of conditionally prepared *single photons* and the entanglement present in PDC *photon pairs*. In the absence of filters, $p = \sum_n\lambda_n^2$, which is equivalent to $p = \dfrac{1}{K}$, where the cooperativity parameter K quantifies the entanglement present in PDC photon pairs. This criterion is a valuable tool for engineering PDC photon-pair sources that are optimized for the generation of pure single-photon wavepackets without resorting to strong filtering. It clearly illustrates the necessity of decoupling the signal and idler photons in all degrees of freedom.

3. SPECTRALLY DECORRELATED TWO-PHOTON STATES

As was shown in Section 2, the generation of pure single-photon wavepackets based on PDC photon pairs necessitates that all spatial–spectral correlations between the signal and idler photons be eliminated. This includes correlations in all degrees of freedom, including spectral, transverse momentum, and polarization. Since the full discussion of all the degrees of freedom is beyond the scope of this paper, for the discussion to follow, we assume that the spatial modes of the PDC photon pairs are independently rendered decorrelated. Such spatial decorrelation can be achieved, for example, by waveguided PDC [5], in which photons are emitted in the form of specific transversely confined modes. In addition, some of the techniques to be presented here that are designed to obtain spectral decorre-

lation for bulk crystals could be extended to the spatial domain.

A number of techniques have been proposed to generate photon pairs exhibiting spectral decorrelation without resorting to spectral filtering. Grice *et al.* showed [11] that a possible avenue towards such states is the group-velocity matching condition derived by Keller *et al.* [12]. Such a technique is extended here, showing that, if an additional condition between the pump chirp and the crystal dispersion is fulfilled, the factorizability of the joint spectral *amplitude* is guaranteed. Considering the complete joint amplitude rather than restricting attention to intensity correlations is important, because correlations in the phase terms of the joint spectral amplitude, which are not apparent in the joint spectral intensity, can introduce correlations in the times of emission. Thus, in order to guarantee full signal–idler pure-state decorrelation, the joint spectral *amplitude* (and, therefore, the joint spectral intensity) must be factorizable.

It has likewise been shown that a spectrally decorrelated state may be obtained by exploiting transverse momentum in a bulk $\chi^{(2)}$ type-I crystal [14]. Specifically, this is achieved using a focused Gaussian pump beam with a spot size fulfilling a certain relationship with the crystal length. Walton *et al.* have recently reported a different scheme, in which a transverse pump generates counterpropagating spectrally decorrelated photon pairs [15]. The essential advantage of these two techniques is that spectral decorrelation may be obtained at any wavelength where phase matching is possible, as opposed to the technique based on group velocity matching, which applies for quite restrictive frequency regimes.

In this paper, we also introduce a novel technique that is based on a sequence of crystals with intermediate birefringent spacers. In this scheme, although group velocities are not matched to each other, the maximum group velocity mismatch observed can be limited to an arbitrarily small value. Furthermore, spectral decorrelation, as well as a more general class of spectrally engineered photon pairs, may be obtained at any wavelength where phase matching for the center wavelengths of the involved pulses is possible.[1]

3.1. Group Velocity Matching

The general expression for the joint probability amplitude of the two-photon state generated in the process of PDC in the ultrashort pulsed-pump regime (and assuming fixed directions of propagation) is given by [8]

$$f(\omega_s, \omega_i) = \alpha(\omega_s, \omega_i)\phi(\omega_s, \omega_i), \qquad (19)$$

[1] Even if birefringent phase matching is not possible, it is usually possible to quasiphase match the process at arbitrary wavelengths.

where $\alpha(\omega_s, \omega_i)$ denotes the pump envelope function and $\phi(\omega_s, \omega_i)$ the so-called phase-matching function. Here, $\alpha(\omega_s, \omega_i)$ is modeled by a Gaussian in terms of the frequency detunings from the central PDC frequency $\nu_\mu = \omega_\mu - \omega_0$:

$$\alpha(\nu_s + \nu_i) = \exp\left[-\left(\frac{\nu_s + \nu_i}{\sigma}\right)^2\right]. \qquad (20)$$

For the phase-matching function $\phi(\omega_s, \omega_i)$, we restrict ourselves to the collinear propagation of the signal and idler photons and assume a plane wave for the pump. If we then define k as the longitudinal component of **k**, the optical properties of the nonlinear crystal with length L determine $\phi(\omega_s, \omega_i)$ as [8]

$$\phi(\omega_s, \omega_i) = \mathrm{sinc}\left(\frac{L\Delta k(\omega_s, \omega_i)}{2}\right)e^{i\frac{L\Delta k(\omega_s, \omega_i)}{2}} \qquad (21)$$

in terms of the phase mismatch

$$\Delta k(\omega_s, \omega_i) = k_s(\omega_s) + k_i(\omega_i) - k_p(\omega_p). \qquad (22)$$

We will at this point restrict our attention to a frequency-degenerate process; i.e., the Taylor expansion for each of the two photons is assumed to be centered at the same frequency, ω_0. We can then express the phase mismatch (Eq. (22)) as a Taylor expansion up to second order:

$$\begin{aligned} L\tilde{k}(\nu_s, \nu_i) &= L\Delta k^0 + \tau_s\nu_s + \tau_i\nu_i \\ &+ \beta_s\nu_s^2 + \beta_i\nu_i^2 + \beta_p\nu_s\nu_i + O(\nu^3), \end{aligned} \qquad (23)$$

with

$$\Delta k^0 = k_s(\omega_0) + k_i(\omega_0) - k_p(2\omega_0) \qquad (24)$$

representing the constant term of the Taylor expansion, which must vanish to guarantee phase matching; $O(\nu^3)$ denotes terms of third and higher order and ($\mu = s, i$)

$$\tau_\mu = L[k'_\mu(\omega_0) - k'_p(2\omega_0)] = L(u_\mu^{-1} - u_p^{-1}),$$

$$\beta_\mu = \frac{L}{2}[k''_\mu(\omega_0) - k''_p(2\omega_0)], \qquad (25)$$

$$\beta_p = -Lk''_p(2\omega_0)$$

are the temporal walkoffs τ_μ between the downconverted and pump pulses (with corresponding group velocities u_μ^{-1} and u_p^{-1}) and the group velocity dispersions β_μ, β_p. In the previous expressions, ' and " indicate first and second derivatives with respect to frequency (evaluated at ω_0 in the case of the signal and idler wave vectors and at $2\omega_0$ in the case of the pump wavevector). u_p represents the pump group velocity, while u_μ ($\mu = s, i$) represents the group velocity experienced by each of the signal and idler photons.

We will use the additional approximation of expressing the sinc function in the phase-matching function as a Gaussian function via the approximation

$$\text{sinc}(x) \approx e^{-\gamma x^2} \quad \text{with} \quad \gamma = 0.193\dots, \quad (26)$$

where the numerical value of γ results from the condition that both functions exhibit the same full-width half-maximum (FWHM) value. We will further allow the pump field to carry a quadratic phase to account for chirp. Under such circumstances, the joint spectral amplitude is given as

$$\tilde{f}(\nu_s, \nu_i) = M \exp\left[-\left(\frac{\nu_s + \nu_i}{\sigma}\right)^2\right]$$

$$\times \exp[i\beta_t(\nu_s + \nu_i)^2] \exp\left[-\frac{\gamma}{4}(\tau_s\nu_s + \tau_i\nu_i)^2\right] \quad (27)$$

$$\times \exp\left[i\frac{1}{2}(\tau_s\nu_s + \tau_i\nu_i + \beta_s\nu_s^2 + \beta_i\nu_i^2 + \beta_p\nu_s\nu_i)\right],$$

where M is a normalization constant and β_t is the group velocity dispersion (GVD) term that the pump experiences prior to the crystal. We note that the above expression contains, within the regime of the approximations used, all terms up to quadratic order in the frequency detunings. By expanding the exponential terms, we can express the joint spectral amplitude as

$$\tilde{f}(\nu_s, \nu_i) \propto \exp\left[-\left(\frac{1}{\sigma^2} + \frac{\gamma}{4}\tau_s^2\right)\nu_s^2\right]$$

$$\times \exp\left[i\frac{\tau_s}{2}\nu_s + i\left(\beta_t + \frac{\beta_s}{2}\nu_s^2\right)\right] \exp\left[-\left(\frac{1}{\sigma^2} + \frac{\gamma}{4}\tau_i^2\right)\nu_i^2\right]$$

$$\times \exp\left[i\frac{\tau_i}{2}\nu_i + i\left(\beta_t + \frac{\beta_i}{2}\nu_i^2\right)\right] \quad (28)$$

$$\times \exp\left[-2\left(\frac{1}{\sigma^2} + \frac{\gamma}{4}\tau_s\tau_i\right)\nu_s\nu_i + i\left(2\beta_t + \frac{\beta_p}{2}\right)\nu_s\nu_i\right].$$

Here, the contributions depending on ν_s and ν_i exclusively, as well as those depending on both ν_s and ν_i, are written as separate factors, and phase terms linear in ν_μ have been dropped. We can see from Eq. (28) that any lack of factorizability resides in the mixed term containing an argument proportional to $\nu_s\nu_i$. Furthermore, we can now easily see that the conditions that guarantee a factorizable state (i.e., that make the mixed term vanish) are

$$\frac{4}{\sigma^2} + \gamma\tau_s\tau_i = 0 \quad (29)$$

and

$$2\beta_t + \frac{\beta_p}{2} = 0. \quad (30)$$

We note that the second condition (Eq. (30)) refers to phase contributions in the joint spectral amplitude and was not included in the earlier work by Grice *et al.* [11]. Because such phase contributions play no role in the intensity, the fulfillment of the first of the derived conditions (Eq. (29)) is sufficient to obtain a factorizable joint spectral *intensity*. If both conditions (Eqs. (29) and (30)) are satisfied, the two-photon state is guaranteed to be free of correlations in the spectral and temporal domains, as indicated by a factorizable joint spectral *amplitude*. We now analyze the effects of the first condition on the two-photon state. If condition Eq. (29) is fulfilled, we may express the joint spectral intensity as

$$S(\nu_s, \nu_i) = \left|\tilde{f}(\nu_s, \nu_i)\right|^2 \propto \exp\left[-2\frac{\nu_s^2}{\sigma_s^2}\right]\exp\left[-2\frac{\nu_i^2}{\sigma_i^2}\right], (31)$$

where the spectral widths σ_s and σ_i are given by

$$\sigma_\mu = \frac{2\sigma}{\sqrt{4 + \gamma\sigma^2\tau_\mu^2}}, \quad (32)$$

with $\mu = s, i$. Thus, we have confirmed that such a joint spectral intensity exhibits the desired factorizability. The ratio of the larger of the two spectral widths (for signal and idler) to the smaller one, which will be referred to as the aspect ratio (i.e., a measure of the degree of elongation exhibited by the two-photon spectral distribution in $\{\omega_s, \omega_i\}$), is given by

$$r = \max\left\{\frac{\sigma_s}{\sigma_i}, \frac{\sigma_i}{\sigma_s}\right\} = \sqrt{\frac{4 + \gamma\sigma^2\tau_1^2}{4 + \gamma\sigma^2\tau_2^2}}, \quad (33)$$

where $\tau_1 = \tau_s$ and $\tau_2 = \tau_i$ if $\sigma_s > \sigma_i$ and, likewise, $\tau_1 = \tau_i$ and $\tau_2 = \tau_s$ if $\sigma_i > \sigma_s$. In what follows, the aspect ratio will prove to be a useful tool in the characterization of the two-photon state.

Let us now consider the effect of the second of the derived conditions (Eq. (30)). We will start by analyzing the effect of the phase terms present in the joint spectral amplitude (Eq. (28)) on the photon pair correlations. First, the linear phases $i\tau_\mu\nu_\mu$ (with $\mu = s, i$) shift the times of emission with respect to the pump pulse for each of the two single-photon wavepackets. For a type-II interaction, $\tau_s \neq \tau_i$ implies that the two single-photon wavepackets forming a given photon pair are emitted at different mean times, where the mean emission time difference is simply $\tau_s - \tau_i$. This temporal walkoff can be compensated by means of a relative delay between the signal and idler photons introduced after the crystal. While the GVD terms (β_s, β_i, and β_p) have no effect on the joint spectral *intensity* of the two-photon state (in the regime of the approximations used, which neglects contributions of cubic and higher order terms in the frequency detunings), they translate into broadening in the temporal domain, which becomes apparent upon carry-

ing out a Fourier transformation of the joint spectral amplitude to obtain the joint temporal amplitude. The quadratic phase $i(\beta_t + \beta_\mu/2)\nu_\mu^2$ (with $\mu = s, i$) results in temporal broadening of the two-photon wavepackets along the time axes (t_s and t_i) independently. The temporal broadening is proportional to the crystal length and is, in general, different for each of the two photons[2] (since $\beta_s \neq \beta_i$). The mixed term, which is proportional to $\nu_s\nu_i$, introduces correlations in the times of emission. This means that a decorrelated behavior in intensity is not sufficient to ensure true single-mode photon-pair generation. We note that it is the β_p term that is responsible for eliminating the factorizability. Therefore, if it were possible to eliminate the effect of β_p, the two-photon joint temporal amplitude would broaden in such a way that the decorrelated character is maintained. Fortunately, it is possible to compensate for the presence of β_p simply by letting the incoming pump field have a chirp (quadratic phase) that fulfills our second derived factorizability condition (Eq. (30)). The quadratic phase that the pump should carry is therefore given by $\beta_t = -\beta_p/4$. We also note that it is in principle possible to "tune" the degree of temporal correlation in the two-photon state (and, therefore, the level of distinguishability in an interference experiment) by using a pump field with a variable chirp, i.e., with a variable β_t.

Let us return to the first of the conditions derived for factorizability (Eq. (29)). This condition may be written in terms of the crystal and pump-field parameters as

$$\frac{4}{\sigma^2} + \gamma L^2 (k_s' - k_p')(k_i' - k_p') = 0, \qquad (34)$$

where σ is the pump bandwidth, L is the crystal length, k_p' represents the first frequency derivative of k_p evaluated at $2\omega_0$, k_μ' ($\mu = s, i$) represents the first frequency derivative of k_μ evaluated at ω_0, and $\gamma \approx 0.193$. For specific experimental situations, pairs of values for the pump bandwidth σ and the crystal length L may exist such that the above condition (Eq. (34)) is fulfilled. Note that, for the condition in Eq. (34) to be fulfilled, one of the following must be true: $k_s' < k_p' < k_i'$ or $k_i' < k_p' < k_s'$; i.e., the group velocity of the pump must lie between that of the signal and idler. None of the experiments recently reported in the literature make use of crystals meeting the above requirements. This should not be surprising, since it requires a material in which one of the daughter photons has a smaller group velocity than the pump, which necessarily has a shorter wavelength. Alternatively, this condition may be expressed as the requirement that τ_s and τ_i have opposite signs.

In order to get further physical insight, consider the phase-matching condition resulting from the approximation of neglecting second- and higher-order terms in the Taylor expansion (and assuming that the constant term vanishes). In this case, the phase-matching condition (see Eq. (22)) becomes

$$\tau_s\nu_s + \tau_i\nu_i = 0. \qquad (35)$$

The contour on the $\{\nu_s, \nu_i\}$-plane defined by perfect phase matching is therefore a straight line with slope $-\tau_s/\tau_i$. In other words, the angle subtended by the ν_s axis and the perfect phase-matching contour is given by

$$\theta_{II} = -\arctan\left(\frac{\tau_s}{\tau_i}\right) = -\arctan\left(\frac{k_s' - k_p'}{k_i' - k_p'}\right), \qquad (36)$$

where the II subscript refers to type-II phase matching. Note that the angle θ_{II} does not depend on the crystal length; it is solely a property of the dispersion of the material at the particular PDC wavelength. For a type-I PDC, $\tau_s = \tau_i$, so that a similarly defined angle has the fixed value $\theta_I = -45°$. Thus, the condition that $k_s' - k_p'$ and $k_i' - k_p'$ have opposite signs cannot be met with a type-I PDC, while, in the case of type-II, it translates into the requirement that the slope of the perfect phase-matching contour be positive.

Let us now consider a specific case fulfilling the positive slope requirement: the case in which the slope of the perfect phase-matching contour is unity; i.e., $\theta_{PM} = 45°$. It is straightforward to show from Eq. (36) that the condition that guarantees such a unit slope is given by

$$\frac{k_s' + k_i'}{2} = k_p', \qquad (37)$$

which says that the average inverse group velocities for the signal and idler photons equal the pump inverse group velocity. This condition, which can be alternatively expressed as $\tau_s + \tau_i = 0$, is referred to as the group velocity matching condition [11, 12]. We can picture this condition as the requirement that the signal and idler photons are temporally delayed with respect to the pump in a symmetric way, with the two PDC photons delayed in opposite directions, by the same amount, from the pump. Alternatively, we may interpret the group velocity matching condition (Eq. (37)) in terms of the joint spectral intensity: when this condition is fulfilled (and when the pump bandwidth is chosen adequately; see [11]), the aspect ratio (see Eq. (33)) evaluates to unity. The latter implies that the factorizable joint spectral intensity exhibits a circular shape on the $\{\nu_s, \nu_i\}$ plane. Such symmetry is crucial for experiments that rely on classical interference between signal and idler PDC modes, since it can then fulfill the requirement of ideal signal–idler spectral-mode matching and lead to unit visibility in the conventional Hong–Ou–Mandel experiment [13]. Hence, in this configuration, the generated PDC two-photon state yields signal–idler mode matching as well as the factorizability

---

[2] In case of a degenerate type-I process, $\beta_s = \beta_i$.

required for conditional preparation of pure single photons, and, therefore, constitutes a versatile two-photon state that is useful for a broad class of experiments [14].

3.2. Asymmetric Group Velocity Matching

In the context exclusively of generating pure single-photon states from separate crystals, each of the crystals used must generate factorizable (but not necessarily symmetric) two-photon states in order to guarantee unit interference visibility in a multicrystal experiment, where signal–signal and idler–idler (but not signal–idler) interference is permitted. Thus, in this context, a nonunit aspect ratio is indeed not a limitation (as long as the elongation is "aligned" with the frequency and time axes). In this section, we study experimental situations in which it is in fact desirable to obtain a state exhibiting a spectrally "elongated" shape and thus a high aspect ratio.

The first condition for frequency decorrelation (Eq. (29)) can in fact be met for several common $\chi^{(2)}$ crystals. For example, in the case of periodically poled KTP (PPKTP) (in degenerate collinear operation), it can be met for configurations where the PDC central wavelength is within the range 1.207 μm < λ < 2.364 μm (see also [16]). Within this range, only the particular wavelength of λ = 1.568 μm fulfills the group velocity matching condition (Eq. (37)), which yields the unit aspect ratio two-photon state, while the aspect ratio departs from unity for all other wavelengths. The lower and upper bounds correspond to two-photon states characterized by a high aspect ratio with asymmetric joint spectral intensities, though they maintain "alignment" with the ν_s and ν_i axes. In [11], it was similarly established that, in the case of BBO, factorizability may be obtained for wavelengths between 1.169 and 1.949 nm with the group velocity matching condition fulfilled at 1.514 nm. This spectral region is of great importance for optical quantum communication using optical fibers. Unfortunately, for the materials discussed above, frequency-decorrelated PDC (and, specifically, unit–aspect ratio decorrelated states) occurs at wavelengths at which single-photon detectors are not well-developed. Although InGaAs avalanche photodiodes have been shown to be capable of photon counting at such longer wavelengths [17], the quantum efficiencies are rather low (about 15%), while dark-count control necessitates cryogenic cooling. Thus, frequency-decorrelated two-photon states, which occur for available crystal materials at longer >1 μm wavelengths, present acute experimental challenges mainly in terms of detection. In what follows, we will discuss the synthesis of factorizable two-photon states in the near-infrared spectral region, which can be accessed more conveniently.

We begin our analysis by rewriting the condition for factorizability (see Eq. (34)) as

$$\frac{4}{\sigma \tau_s} + \gamma \sigma \tau_i = 0. \qquad (38)$$

We consider this condition in the long PDC crystal regime. Recall that the temporal walkoff terms τ_s and τ_i are each proportional to the crystal length L. Thus, we see that, if $\tau_s \gg \sigma^{-1}$ (as is the case in the limit $L \longrightarrow \infty$), the condition reduces to the following simpler constraint: $\tau_i = 0$; i.e., the latter tells us that spectral decorrelation can be achieved by employing a long crystal while making one of the temporal walkoff terms vanish. Since in this variant of the technique the pump group velocity is matched to that of one of the PDC photons (but not to both), we refer to this technique as asymmetric group velocity matching. Note that, for a given crystal length L, the frequency decorrelation condition (Eq. (34)) can in general be met at most for isolated values (usually not more than one) of the pump bandwidth σ; i.e., there is a strict one-to-one relationship between crystal length L and the pump bandwidth σ required for spectral factorizability. The latter can be an experimental limitation if, for example, the pump bandwidth cannot be easily modified. In the long crystal regime, however, the condition becomes independent of the pump bandwidth σ. The fact that a frequency-decorrelated two-photon state may thus be synthesized irrespective of the pump bandwidth makes such a long crystal PDC a more flexible source of spectrally engineered photon pairs. In such a long-crystal source, varying the pump bandwidth merely alters the aspect ratio without affecting the spectral decorrelation.

Fortunately, it is possible to obtain a decorrelated two-photon state (albeit with a high aspect ratio) at wavelengths suitable for room-temperature-operated silicon-based avalanche photodiodes. Such detectors exhibit both a ~60% quantum efficiency (in the near-infrared spectral region) and a manageable level of dark counts. Figure 1 shows a two-photon state produced by collinear degenerate type-II PDC in a 2-cm-long KDP crystal cut at a phase-matching angle of 68°, yielding photon pairs centered at 830 nm. Note that, although the spectral distribution is elongated, factorizability is exhibited and, hence, conditional pure-state generation (see Section 2) is ensured. It is also interesting to notice that, in contrast to general PDC photon pairs, such a state is predicted to yield conditionally prepared photon states that are Fourier-transform-limited [18]. The two-photon state features a narrow spectrum for the ordinary-ray photon and a broader one for the extraordinary-ray photon. This arises from the matching of the group velocity of the pump photons to that of the o-ray photon (but not to the e-ray photon).

In summary, our proposed long-crystal KDP-source, yielding spectrally factorizable photon pairs based on asymmetric group velocity matching, is characterized by the following properties: (1) If it is used for
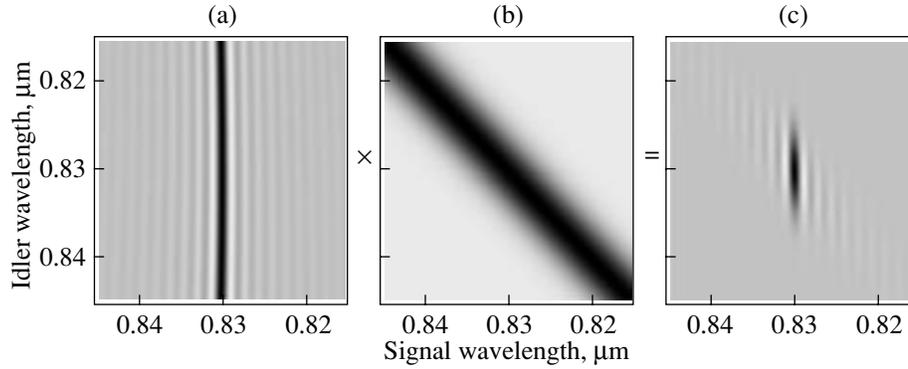
Fig. 1. High-aspect-ratio decorrelated two-photon state obtained by degenerate collinear PDC from a 2-cm-long KDP crystal exhibiting a cut angle of 68°. (a) "Vertical" phase-matching function $\phi(\omega_s, \omega_i)$ exhibiting asymmetric group velocity matching. (b) Pump-envelope function describing a Fourier-transform-limited pump pulse centered at 415 nm with a spectral bandwidth of 5 nm. (c) Resulting nearly factorizable two-photon state.

conditional single-photon generation, the prepared photons are described by quantum-mechanically pure states. This property is evident in the Fourier-transform-limited character of the photonic wavepackets. (2) The narrow spectral bandwidth of the ordinary-ray photons allow spectral filtering to eliminate any background light without discarding PDC photons. If the filtered mode is then used as a trigger in a conditional source of single photons, the resulting prepared photon exhibits the largest spectral bandwidth allowed by the pump bandwidth. (3) Assuming that the spectral bandwidth of the pump is large enough that the phase-matching function dominates over the pump-envelope function, the decorrelated character is independent of the pump bandwidth, thus eliminating an important experimental constraint. (4) The generated state requires a pump centered at 415 nm, which is easily accessible with a frequency-doubled titanium:sapphire laser, while the produced photons at 830 nm can be efficiently detected with silicon-based single-photon-counting modules. Even though KDP has a smaller nonlinearity than other common $\chi^{(2)}$ materials such as BBO, the long crystal used translates into a gain in the production rate of photon pairs with respect to typical PDC sources that are based on shorter crystals. (5) KDP crystals at a ~70° cut angle exhibit a relatively small transverse walkoff; at a pump wavelength of 415 nm, the walkoff angle is 1.15°, which gives, for a 2-cm-long crystal, a lateral displacement of just over 400 μm. We note, however, that, used as a conditional source of single photons in networks where signal and idler modes are not superimposed, the walkoff exhibited is not a limitation, as the signal and idler photons need not be indistinguishable from each other. (6) As will be discussed in the next section, such a high-aspect-ratio factorizable state additionally exhibits an interesting dispersion-insensitivity effect.

3.3. Dispersion Insensitivity in Long-Crystal Asymmetrically Group-Velocity-Matched Photon Pairs

As was discussed above, broadening of the joint spectral amplitude results from GVD terms that (see Eqs. (25)) are proportional to the crystal length. Thus, increasing the crystal length used leads to a temporally broader two-photon time of emission distribution. If the mixed-term phase $2\beta_t + \dfrac{\beta_p}{2}$ in Eq. (28) does not vanish, such broadening eliminates the "alignment" with the time axes. However, in this section we will show that, for high-aspect-ratio spectrally factorizable two-photon states, in the long-crystal regime the mixed term responsible for introducing correlations in the times of emission can be made arbitrarily small (even though temporal broadening still occurs for each of the two photons independently). In fact, an increase in crystal length gives a net reduction of temporal correlations.

Let us assume that the crystal length and pump bandwidth are chosen so that the first condition for factorizability (Eq. (29)) is satisfied. Under these circumstances (see Eq. (31)), the joint spectral amplitude may be expressed as

$$f(\omega_s, \omega_i) = \exp\left[-\frac{\nu_s^2}{\sigma_s^2}\right]\exp\left[-\frac{\nu_i^2}{(r\sigma_s)^2}\right] \qquad (39)$$

$$\times \exp[i(\beta_s\nu_s^2 + \beta_i\nu_i^2 + \beta_p\nu_s\nu_i)],$$

where we have expressed the idler width in terms of the aspect ratio r as $\sigma_i = r\sigma_s$ and where the GVD terms (β_s, β_i, and β_p) were defined in Eq. (25). Note that, since the lack of factorizability in the above expression resides in the phase term, the joint spectral *intensity* is factorizable. Nevertheless, the presence of a mixed-phase term that is proportional to β_p translates into a lack of factorizability in the temporal domain. In order to study the temporal properties of the wavepacket, let us carry out

a Fourier transform of the above joint spectral amplitude to obtain the following joint temporal intensity:

$$\mathcal{S}(t_s, t_i) = |\mathcal{F}(t_s, t_i)|^2$$
$$= \exp\left[-\frac{2t_s^2}{\delta t_s^2}\right]\exp\left[-\frac{2t_i^2}{\delta t_i^2}\right]\exp[-2\sigma_M^2 t_s t_i], \quad (40)$$

where the temporal wavepacket width along t_s is given in terms of the reciprocal aspect ratio $s = r^{-1}$ by

$$\delta t_s = \frac{2\sqrt{2}\sqrt{2 + \sigma_s^4(2\beta_s^2 + \beta_p^2 s^2 + 2\beta_i^2 s^4)}}{\sigma_s\sqrt{4 + \sigma_s^4 s^2(\beta_p^2 + 4\beta_i^2 s^2)}}, \quad (41)$$

the temporal wavepacket width along t_i is given by

$$\delta t_i = \frac{2\sqrt{2}\sqrt{2 + \sigma_s^4(2\beta_s^2 + \beta_p^2 s^2 + 2\beta_i^2 s^4)}}{s\sigma_s\sqrt{4 + \sigma_s^4(4\beta_s^2 + 4\beta_p^2 s^2)}}, \quad (42)$$

and

$$\sigma_M^2 = \frac{\sigma_s^6 s^2 \beta_p(\beta_s + \beta_i s^2)}{2(2 + \sigma_s^4(2\beta_s^2 + \beta_p^2 s^2 + 2\beta_i^2 s^4))} \quad (43)$$

represents the mixed-term coefficient. Specializing to a high-aspect-ratio spectrally factorizable state, such as one produced by the long KDP crystal source discussed in the last section, the temporal walkoff τ_0 between the pump and the ordinary-ray photon vanishes. Thus, according to Eq. (32), the ordinary-ray spectral width is then given by $\sigma_s = \sigma$, where σ represents the pump bandwidth. Likewise, in the long-crystal limit, according to Eq. (32), the idler spectral width is given by $1/(\sqrt{\gamma}\tau_e)$. This leads to the following expression for the reciprocal aspect ratio $s = r^{-1}$:

$$s = \frac{2}{\sqrt{\gamma}\sigma(k_s' - k_p')L}. \quad (44)$$

Note from the above expression that the reciprocal aspect ratio s is inversely proportional to the crystal length L. This fact, together with the linear dependence of each of the GVD terms (β_s, β_i, and β_p) on the crystal length L can be used to express the mixed-term coefficient σ_M^2 in terms of its overall length dependence. We thus obtain

$$\sigma_M^2 \approx \frac{\sigma^6 s^2 \beta_p \beta_s}{4(1 + \sigma^4 \beta_s^2)}$$
$$= \frac{\sigma^4 k_p'(k_s' - k_p')}{4\gamma(k_i' - k_p')^2[1 + \sigma_p^4 L^2(k_s' - k_p')^2]}. \quad (45)$$

The net crystal-length dependence of σ_M^2 in the long-crystal regime is inverse quadratic. Hence, increasing

the crystal length not only does lead to an increase in the magnitude of the mixed term but actually reduces the time-of-emission correlations. Recall that, for a factorizable high-aspect-ratio two-photon state, the pump bandwidth σ and crystal length L need not be specified jointly; i.e., there is no relationship that should be fulfilled between them to ensure factorizability. Together with the dispersion-insensitivity effect discussed here, the latter means that the crystal can be made arbitrarily long without introducing temporal correlations. The main remaining considerations using a long crystal are excessive temporal broadening and absorption of PDC photons in the crystal. We note that, if the pump field is chirped, β_p should be substituted by $2\beta_t + \frac{\beta_p^2}{2}$ in the expressions for the mixed term (Eqs. (43) and (45)) (where β_t was introduced in Eq. (28) and represents the quadratic phase carried by the pump field). The presence of chirp in the pump pulse can be treated similarly: upon increasing the crystal length L, the magnitude of the mixed term decreases. Thus, we conclude that (within the regime of validity of the approximations used) the source presented here is insensitive to those dispersive effects, leading to the appearance of temporal correlations that are either introduced in the PDC crystal itself or, indeed, prior to the crystal.

We can understand the dispersion-insensitivity effect described above by realizing that dispersion effects in general require not only the presence of a dispersive phase but also broadband light. Engineering the joint spectral intensity by making it nearly monochromatic along either the signal or the idler axis means that the resulting narrowband photon will experience limited dispersion, as manifest in the reduction of the mixed term σ_M. Figure 2 shows the two-photon state produced by collinear degenerate type-II PDC in a 2-cm-long KDP crystal cut at a phase-matching angle of 68° and yielding photon pairs centered at 830 nm. The joint *spectral* intensity is shown in Fig. 2a, while the joint *temporal* intensity is shown in Fig. 2b. Because the parameters of the source fulfill Eq. (34), the joint spectral intensity is factorizable. Furthermore, the joint temporal intensity is also factorizable for arbitrarily long crystals. Thus, the two-photon state produced by such a two-photon source is free from spectral (temporal) correlations, making it an ideal source of conditionally prepared pure and Fourier-transform-limited single-photon wavepackets.

4. TWO-PHOTON-STATE ENGINEERING VIA CRYSTAL SEQUENCES WITH BIREFRINGENT COMPENSATORS

As has been shown in this paper, group velocity matching is a powerful technique, one which enables the engineering of two-photon states with desirable properties that are tailored for specific applications. Nevertheless, group velocity matching crucially
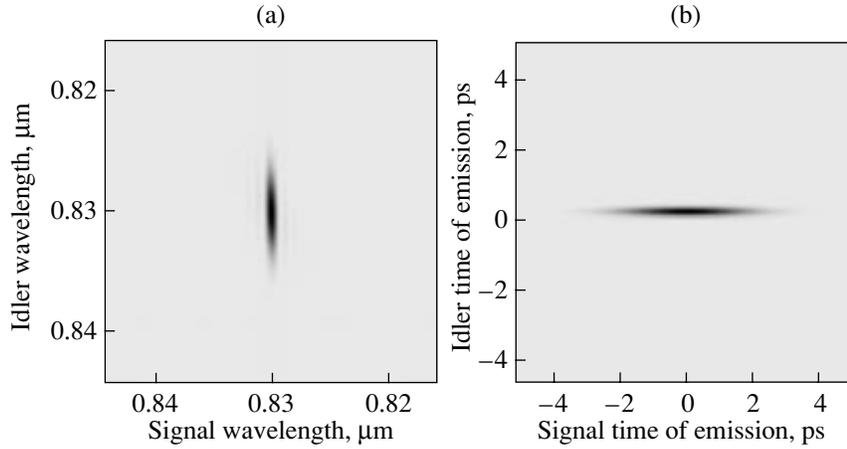
Fig. 2. High-aspect-ratio two-photon state obtained by degenerate collinear PDC of a pump pulse of approximately 100-fs duration at 415 nm in a 2-cm-long KDP crystal. The state exhibits space–time decorrelation. (a) Factorable joint *spectral* intensity; (b) factorable joint *temporal* intensity.

depends on the dispersion exhibited by the pump, signal, and idler fields in the nonlinear crystal used and tends to occur only in specific wavelength ranges. In this section, we propose and analyze a technique in which the group velocity mismatch can be controlled, in principle, at arbitrary wavelengths. This comes at the cost, however, of an increased source complexity. In this scheme, a *sequence* of nonlinear crystals is used, which is interspersed with birefringent spacers exhibiting a dispersion such that the group velocity mismatch introduced by the crystal is compensated for by that in the spacer. This scheme can be thought of as analogous to bandgap engineering using photonic crystals, except that group velocity, rather than phase velocity, is compensated.

Consider the experimental arrangement shown in Fig. 3, which consists of N identical $\chi^{(2)}$ crystals and $N - 1$ linear optical $\chi^{(1)}$ spacers. Each of the crystals is assumed to be cut and oriented for a degenerate collinear type-II PDC, while the compensators are assumed not to exhibit a $\chi^{(2)}$ nonlinearity. It is further assumed that each crystal has length L, while each spacer has length h. The phase mismatch in each of the crystals is given by

$$\Delta k = k_p - k_s - k_i, \tag{46}$$
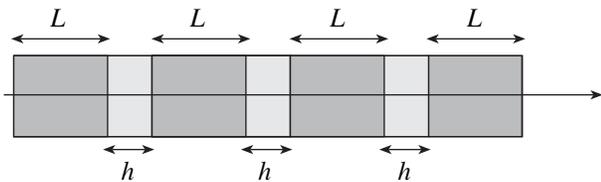
Fig. 3. Schematic of the proposed crystal sequence with intermediate birefringent spacers. Each crystal has a length L, while each spacer has a length h.

where k_μ (with $\mu = p, s, i$) denotes the wavenumber for each of the three fields taking into account dispersion in the crystal. The phase mismatch introduced by each of the spacers is equivalently given by

$$\Delta\kappa = \kappa_p - \kappa_s - \kappa_i, \tag{47}$$

where κ_μ (with $\mu = p, s, i$) now represents the wavenumber for each of the three fields, taking into account dispersion in the birefringent spacer. For an assembly of N crystals and $N - 1$ spacers, the overall phase-matching function can then be calculated as

$$
\begin{aligned}
\phi_N(\Delta k, \Delta\kappa) &= \sum_{m=0}^{N-1} e^{im(L\Delta k + h\Delta\kappa)} \mathrm{sinc}\left[\frac{L}{2}\Delta k\right] \\
&= e^{\frac{i(N-1)\Phi}{2}} \frac{\sin\left(\frac{N\Phi}{2}\right)}{\sin\left(\frac{\Phi}{2}\right)} \mathrm{sinc}\left[\frac{L\Delta k}{2}\right],
\end{aligned} \tag{48}
$$

where we have defined the quantity Φ as

$$\Phi = L\Delta k + h\Delta\kappa. \tag{49}$$

Hence, apart from an overall phase factor, the crystal assembly phase-matching function is composed of the product of two distinct functions: one corresponds to the phase-matching function of a single crystal, and the second factor incorporates the combined effect of the crystal and spacer dispersion. In order to carry out more explicit calculations, it is helpful to write down the crystal and spacer phase mismatch as a Taylor expansion (similar to that in Eq. (23); however, here we omit all terms of orders higher than $O(\nu^2)$). Thus, we obtain, in terms of the frequency detunings $\nu_\mu = \omega_\mu - \omega_0$ (with $\mu = s, i$),

$$\Phi = L\Delta k^{(0)} + h\Delta\kappa^{(0)} + T_s\nu_s + T_i\nu_i, \tag{50}$$

where $L\Delta k^{(0)}$ and $h\Delta\kappa^{(0)}$ denote the constant terms of the Taylor expansions for the crystal and spacer phase-mismatch terms and where

$$T_\mu = [k'_p(2\omega_0) - k'_\mu(\omega_0)]L + [\kappa'_p(2\omega_0) - \kappa'_\mu(\omega_0)]h \quad (51)$$

with $\mu = s, i$ represent the first-order coefficients of the expansion. The term $\Delta k^{(0)}$ vanishes under the assumption that each of the crystals is aligned such that phase matching is attained.

We can now analyze the influence of the proposed crystal and birefringent compensator assembly on the joint spectral correlations and introduce a new function

$$\Upsilon_N(x) = \frac{1}{N}\frac{\sin(Nx)}{\sin(x)}, \quad (52)$$

which describes the modifications to the spectral structure of the phase-matching function (see Eq. (48)). As depicted in Fig. 4, the function $\Upsilon_N(x)$ exhibits for large values of N a periodic structure of narrow peaks that are separated by 2π. While for odd values of N all peaks are positive, for even values of N the peaks alternate between positive and negative values. The width of the peaks diminishes with increasing N. We may thus write the resulting phase-matching function (where the phase term in Eq. (48) is to be neglected) for the crystal assembly as

$$\phi_N(\nu_s, \nu_i) = \phi(\nu_s, \nu_i)\chi(\nu_s, \nu_i; N), \quad (53)$$

where $\phi(\nu_s, \nu_i)$ represents the *single-crystal* phase-matching function and $\chi(\nu_s, \nu_i; N)$ the crystal assembly contribution. If we express the phase mismatch as a Taylor series, considering only terms up to the first order we obtain, for the phase-matching function, the crystal assembly contribution

$$\chi(\nu_s, \nu_i; N) = \Upsilon_N\left(\frac{1}{2}[h\Delta\kappa^{(0)} + T_s\nu_s + T_i\nu_i]\right) \quad (54)$$

and the single-crystal contribution

$$\phi(\nu_s, \nu_i) = \text{sinc}\left[\frac{L}{2}(\tau_s\nu_s + \tau_i\nu_i)\right], \quad (55)$$

where the τ_μ values are similar to T_μ (with $\mu = s, i$) (see Eq. (51)), except for the absence of a spacer dependence

$$\tau_\mu = [k'_p(2\omega_c) - k'_\mu(\omega_c)]L. \quad (56)$$

Let us now study the increased flexibility introduced into the two-photon state by such a proposed crystal–spacer assembly. We start our analysis by noting that the contours of the $\chi(\nu_s, \nu_i; N)$ function are straight lines with a slope given by

$$\tan\theta = -\frac{T_s}{T_i} = -\frac{(k'_p - k'_i)L + (\kappa'_p - \kappa'_i)h}{(k'_p - k'_s)L + (\kappa'_p - \kappa'_s)h}. \quad (57)$$

Unlike for the case of a single crystal, where a change in crystal thickness merely results in an alteration of the
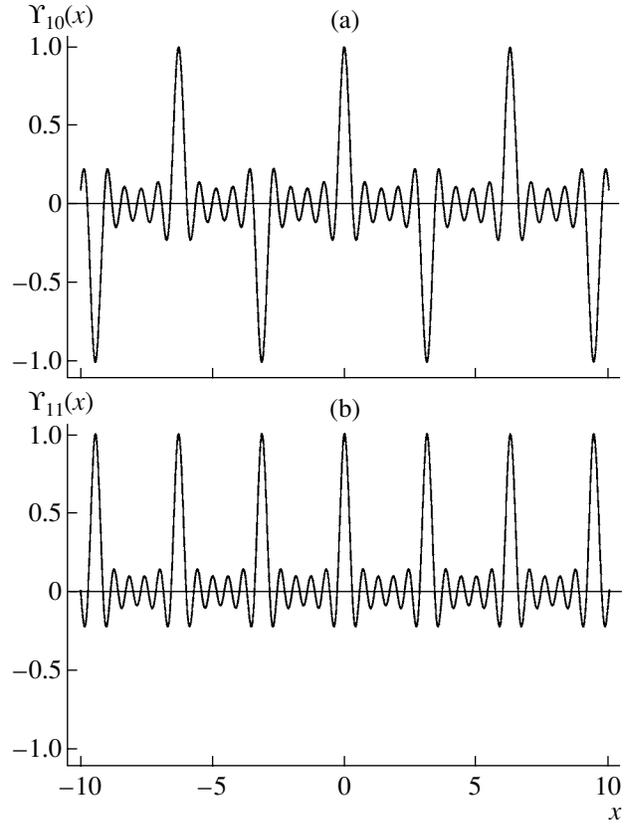
Fig. 4. Plots of the $\Upsilon_N(x)$ function showing different behavior for even and odd N; while for even N peaks alternate with valleys (separated by π), for odd N there are no valleys. The peaks and valleys become narrower with increasing N. Such a function describes the phase-matching contribution from the crystal birefringent spacer sequence.

spectral width (and further modifications to the phase-matching function cannot be attained except by using different spectral regions or by using different crystal materials), in the case of our crystal sequence source the orientation of the spectral phase-matching structure can be adjusted at will by varying the crystal-to-spacer thickness ratio L/h. The latter represents a very important added flexibility, as it means that in principle an arbitrary orientation for the phase-matching-function orientation can be obtained.

To illustrate the power of such PDC engineering, we will discuss below the specific case of synthesizing a phase-matching function with unit slope contours. As was seen in Section 3.1 (see also [11]), such a unit slope can result in spectrally decorrelated two-photon states. For the crystal assembly, the inverse group velocities k'_μ, κ'_μ (with $\mu = i, j$) evaluated at ω_0 and k'_p, κ'_p evaluated at $2\omega_0$, as well as the lengths L and h, should all satisfy the condition

$$(k'_s + k'_i - 2k'_p)L + (\kappa'_s + \kappa'_i - 2\kappa'_p)h = 0. \quad (58)$$

Equation (58) closely resembles the group velocity matching condition (see Eq. (37)). In fact, this condition tells us that unit-slope phase-matching contours require that a generalized group velocity condition be fulfilled: the weighted average (with crystal and spacer lengths as weighting factors) of the group velocity mismatch in the crystal and the spacer must vanish. Note that, for this condition to be attainable, the spacer must exhibit a group velocity mismatch with the opposite sign from that of the crystal itself. A second condition that must be fulfilled relates to the constant phase term $h\Delta\kappa^{(0)}$ (see Eq. (50)). If such a term differs from a multiple of 2π, the maxima of the $\Upsilon_N(x)$ function can shift away from degeneracy (indeed, by tuning such constant phase term, the resulting modes shift on the $\{\nu_s, \nu_i\}$ plane). Thus, a second condition on the spacer length that must be met is as follows:

$$h = \frac{2\pi m}{\Delta\kappa^{(0)}}, \qquad (59)$$

with m being an integer number. This tells us that the spacer length should be given as an integer multiple of the minimum allowed spacer thickness $2\pi/\Delta\kappa^{(0)}$. Thus, if the conditions expressed by Eqs. (58) and (59) are fulfilled, the crystal assembly phase-matching function can be written as

$$\chi(\nu_s, \nu_i; N) = \Upsilon_N(T_-[\nu_s - \nu_i]), \qquad (60)$$

where

$$T_- = \frac{1}{2}([k_s'(\omega_0) - k_i'(\omega_0)]L + [\kappa_s'(\omega_0) - \kappa_i'(\omega_0)]h). \quad (61)$$

Such a function consists of "ridges" (alternated with "trenches" for even N) described by unit-slope contours with a FWHM (along the $\nu_s - \nu_i$ direction) that is given in the limit of large N by

$$\delta\lambda = \frac{\sqrt{2}\lambda_0^2\gamma_2}{\pi c N T_-}, \qquad (62)$$

with $\gamma_2 = 1.39156...$ (this numerical value results from calculating the width of the $\Upsilon_n(x)$ function in the large-N limit) and where λ_0 denotes the central PDC wavelength. The maxima of different "ridges" result from the argument of the Υ_N, yielding multiples of 2π. In the case studied here, where group velocity matching is attained (see Eq. (58)), the spectral separation between subsequent ridges along the $\nu - \nu_i$ direction can be shown to be given by

$$\Delta\lambda = \frac{\lambda_0^2}{\sqrt{2}cT_-}. \qquad (63)$$

Note that the generation of a spectrally decorrelated state actually necessitates a source with a single "ridge"; multiple ridges yield a joint spectral intensity with multiple peaks in $\nu_s - \nu_i$ space, which precludes

spectral factorizability. Because a single ridge is not attainable with our crystal–spacer assembly source, we aim to let the separation between subsequent ridges be as large as possible, so that the portion of the quantum state exhibiting the desired behavior can be isolated, e.g., by weak spectral filtering. We would like to emphasize that such spectral separation between subsequent ridges $\Delta\nu$ is inversely proportional to the parameter T_-, which in turn is proportional to the two thicknesses L and h. This leads to the manufacturing constraint that the individual crystal and spacer lengths should be as short as possible. As will be shown below, this technique can indeed lead to a source of a decorrelated state with experimentally feasible crystal and spacer thicknesses.

Altogether, the resulting joint spectral amplitude for the two-photon state produced by such a crystal assembly is therefore given by

$$f(\nu_s, \nu_i) = \alpha(\nu_s + \nu_i)\phi(\nu_s, \nu_i)\chi(\nu_s, \nu_i; N), \quad (64)$$

where $\alpha(\nu_s + \nu_i)$ represents the pump-envelope function, which will be modeled as a Gaussian, as in Eq. (20). Our approach is to let the bandwidth of the single-crystal phase-matching function $\phi(\nu_s, \nu_i)$ be much larger than that of the function $\chi(\omega_s, \omega_i; N)$ that results from the crystal assembly. Thus, the spectral structure imposed on the phase-matching function by the crystal assembly dominates over that of a single crystal. Given that the bandwidth of individual ridges of the function $\chi(\nu_s, \nu_i; N)$ depends inversely on N (while that of the function $\phi(\nu_s, \nu_i)$ does not depend on N), it is possible, simply by using a sufficiently large number of crystals, to ensure that this condition on the widths of these two functions is fulfilled. Let us note that, for the case of interest, i.e., when the generalized group velocity matching condition (see Eq. (58)) is satisfied, the orientations of $\chi(\nu_s, \nu_i; N)$ and that of the pump-envelope function are orthogonal to each other (along the $\nu_s + \nu_i$ and $\nu_s - \nu_i$ directions, respectively). This leads to the important conclusion that, by choosing the pump bandwidth appropriately, a factorizable two-photon state can be obtained that exhibits nearly circular contours in the $\{\nu_s, \nu_i\}$ plane. The value for the pump bandwidth σ, which guarantees such factorizable behavior, can be expressed in terms of the number of crystal segments N and the parameter T_- (see Eq. (61)) as

$$\sigma = \frac{2\sqrt{2}}{\sqrt{\ln(2)}}\frac{\gamma_2}{NT_-}. \qquad (65)$$

In summary, the proposed strategy for synthesizing a decorrelated two-photon state is as follows: (i) The crystal and spacer materials should be chosen such that the group velocity mismatch for the crystal and spacer material have opposite signs. (ii) The crystal and spacer thicknesses L and h should be chosen so that the generalized group velocity matching condition (see Eq. (58)) is fulfilled and such that the constant phase term $h\Delta\kappa^{(0)}$
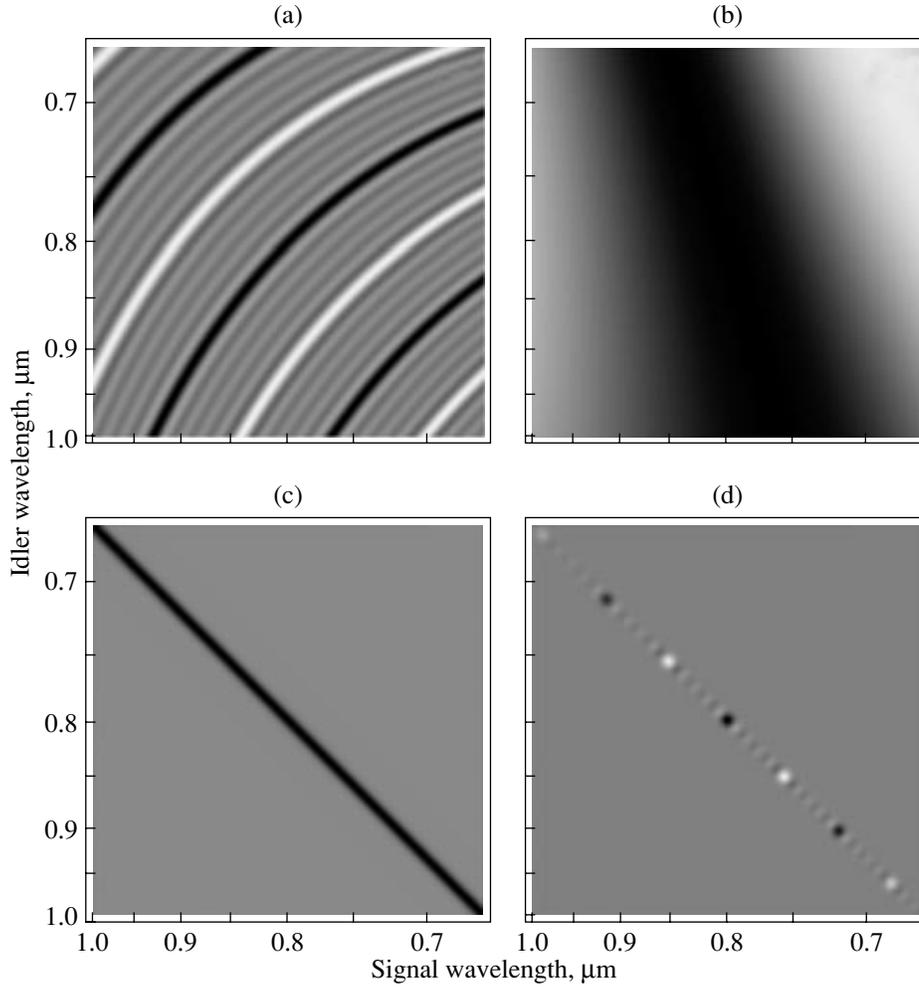
Fig. 5. (a) Assembly contribution to the phase-matching function for the case of ten BBO crystals with a cut angle of $\theta_c = 42.35°$ (each with a thickness of 48.85 μm) alternated with nine calcite spacers (each with a thickness of 58.83 μm). Black areas indicate positive values, while white areas indicate negative values. (b) Phase-matching function for single BBO crystal with the above characteristics. (c) Pump-envelope function for a pump field centered at 400 nm with a bandwidth of 1.48 nm. (d) Resulting joint spectral amplitude function.

yields a multiple of 2π (see Eq. (59)). Additionally, the crystal and spacer should be thin enough that the spectral separation between modes of the $\chi(\nu_s, \nu_i; N)$ function is large enough to ensure that a single resulting mode may be isolated. (iii) The number of crystal segments N should be made large enough that the phase-matching bandwidth of a single crystal is much larger than that of the assembly phase-matching function $\chi(\nu_s, \nu_i; N)$. (iv) The pump should be prepared so that it exhibits a bandwidth σ that fulfills Eq. (65), thus guaranteeing that the pump-envelope and phase-matching functions are such that they yield a factorizable two-photon state.

We now study a specific example involving an assembly of BBO crystals and calcite spacers. Each of the crystals is characterized by a cut angle of $\theta_c = 42.35°$, yielding type-II collinear degenerate phase matching at a central PDC wavelength of $\lambda_c = 800$ nm.

We remark that BBO and calcite exhibit the required opposite-sign group velocity mismatch; for BBO, $2k'_p - k'_s - k'_i = 3.535 \times 10^{-4}$ ps/μm, whereas for calcite, $2\kappa'_p - \kappa'_s - \kappa'_i = -2.936 \times 10^{-4}$ ps/μm.[3] The generalized group velocity matching condition (see Eq. (58)) tells us that the ratio of the calcite spacer thickness to the BBO crystal thickness should be $h/L = 1.204$. This yields a value for the minimum spacer thickness of $2\pi/\Delta\kappa^{(0)} = 5.88$ μm; we choose a value for the integer m (see Eq. (59)) of $m = 10$, thus yielding a spacer thickness $h = 58.83$ μm and a BBO crystal thickness $L = 48.85$ μm. These thicknesses yield a spacing between assembly phase-matching modes (along the $\nu_s - \nu_i$ direction) of $\Delta\lambda = 67.05$ nm, corresponding to a separation along the ν_s or ν_i axes of 47.41 nm. The latter

---

[3] Note that this behavior occurs for a particular orientation of the calcite spacers.
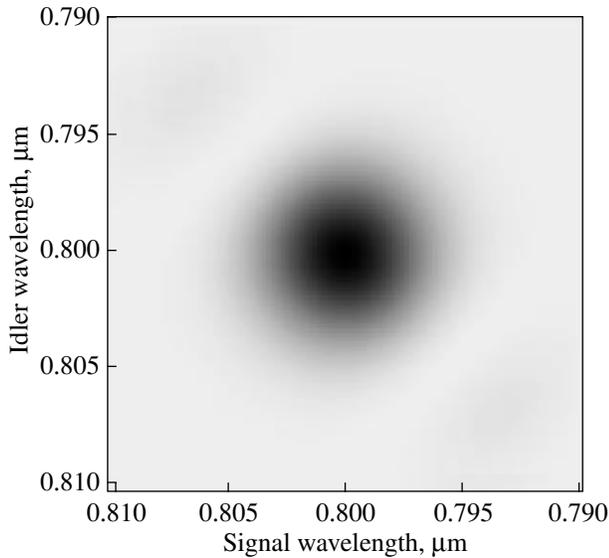
Fig. 6. Joint spectral intensity of the two-photon state produced by a sequence of ten BBO crystals and nine calcite spacers, as was discussed in the text. The plot shows the region of the main degenerate peak near $\lambda_s = \lambda_i = 800$ nm.

means that, over a bandwidth of ~95 nm around the central PDC wavelength (of 800 nm), there is a single-crystal–spacer assembly phase-matching mode present. Figure 5a shows a plot of the function $\chi(\nu_s, \nu_i; 10)$ for the above parameters, i.e., assuming that the assembly contains ten BBO crystals and nine calcite spacers. Note that, near degeneracy (at $\lambda = 800$ nm), the slope of the contours defining the function is indeed unity. Figure 5b shows a plot of the phase-matching function $\phi(\nu_s, \nu_i)$ for a single BBO crystal (with the above characteristics), making it clear that the spectral bandwidth exhibited is much larger than that of the assembly phase-matching modes; the latter implies that the overall phase-matching spectral structure is dominated by the assembly rather than the single-crystal contribution. Figure 5c shows the pump-envelope function corresponding to a pump field with a center wavelength of 400 nm and a spectral FWHM of 1.48 nm, as required by Eq. (65) to yield a factorizable state. Figure 5d shows the resulting joint spectral amplitude for our crystal assembly source. Due to the periodic character of the Υ_N function, there are multiple modes, which are separated along each frequency axis by 47.4 nm. Nevertheless, weak spectral filtering can isolate the central mode (centered at $\lambda_s = \lambda_i = 800$ nm). Figure 6 shows the joint spectral intensity corresponding to this central mode, which clearly exhibits spectral decorrelation.

We have presented a novel technique, based on group velocity matching compensation using a sequence of crystal segments alternated with birefringent spacers, that can yield factorizable states. The essential advantage of this approach is that it becomes, in principle, possible to synthesize a wide class of two-

photon states simply by varying the spacer-to-crystal thickness ratio, while choosing the crystal and spacer materials so that they obey certain relative dispersive properties. This scheme does not altogether eliminate the need for filtering; however, by reducing the crystal and spacer thicknesses L and h (and thus increasing $\Delta\lambda$; see Eq. (63)), it becomes possible to increase the separation between modes, ideally to the point where, in practice, a single mode is present. In the example shown above, the thicknesses were chosen in the region of 50 μm, since thinner segments may be difficult to manufacture and to handle. Moreover, the tolerance of the linear spacer thicknesses becomes more restrictive for larger assemblies. In the example given above, the spacer-thickness error tolerance is about 2%, in order to give a peak at the specified wavelengths that has sufficient isolation for filtering. The tolerances are less restrictive for lower-order structures (i.e., those with smaller values of N). However, it is possible that, by doping, ion exchange, or some other process, a single crystal may be modified in certain regions in such a manner that the group velocity mismatch changes sign; the modified regions would then play the role of the spacers, however, in a single monolithic structure. With this approach, it may be possible to take advantage of the smallest thicknesses allowed (with a value of $m = 1$ in Eq. (59)) and thus eliminate the challenges likely to be faced in assembling a large number of thin crystals.

5. CONCLUSIONS

We have studied single-photon conditional preparation based on photon pairs generated by the process of parametric downconversion. By modeling the detection as an appropriately defined projection operator, we showed that, in general, the quantum state of the prepared state is described as a statistical mixture of the modes defined by the Schmidt decomposition of the PDC two-photon state. Furthermore, it was determined that a two-photon state that has strictly correlated photon numbers but that lacks correlations between the signal and idler photons in all spatial–spectral degrees of freedom is a basic requirement for ideal single-photon preparation, i.e., for yielding quantum-mechanically pure single photons. Such pure single-photon wave-packets are of fundamental importance in experiments relying on quantum interference of single photons from distinct sources, as is the case in the recently proposed scheme for quantum computation with linear optics [4].

Assuming that spatial correlations can be independently eliminated (for example, by the use of a waveguided PDC [5]), we have discussed two techniques that result in spectrally factorizable two-photon states. First, it was shown that, if an additional condition on the two-photon state is fulfilled, the technique reported by Grice *et al.* [11] can yield a state in which both the joint *temporal* intensity and the joint *spectral* intensity are factorizable. The latter is crucial to guaranteeing full factorizability in two-photon states

designed for the conditional preparation of pure single photons. Secondly, we have introduced a novel technique in which the group velocity mismatch between the pump and downconverted photons, which is responsible for the mixed nature of the prepared single photons, can be controlled by using a sequence of crystals alternated with birefringent spacers exhibiting a dispersion that compensates that of the crystal in a specific manner. This represents a powerful technique, in which spectrally decorrelated states, as well as a more general class of spectrally engineered two-photon states, can be obtained simply by varying the relative thicknesses of the crystal and spacer used. These techniques may provide useful tools for practical implementations of novel quantum-enhanced technologies, such as linear optical quantum computation.

ACKNOWLEDGMENTS

REFERENCES

1. D. Bouwmeester *et al.*, Nature **390**, 575 (1997); D. Boschi *et al.*, Phys. Rev. Lett. **80**, 1121 (1998).

2. K. Mattle, H. Weinfurter, P. G. Kwiat, and A. Zeilinger, Phys. Rev. Lett. **76**, 4656–4659 (1996).

3. N. Gisin, G. G. Ribordy, W. Tittel, and H. Zbinden, Rev. Mod. Phys. **74**, 145 (2002).

4. E. Knill, R. LaFlamme, and G. J. Milburn, Nature **409**, 46 (2001); T. C. Ralph, A. G. White, W. J. Munro, and G. J. Milburn, Phys. Rev. A **65**, 012 314 (2001); T. B. Pittman, M. J. Fitch, B. C. Jacobs, and J. D. Franson, quant-ph/0303095 (2003).

5. A. B. U'Ren, C. Silberhorn, K. Banaszek, and I. A. Walmsley, Phys. Rev. Lett. **93**, 093 601 (2004).

6. U. M. Titulaer and R. J. Glauber, Phys. Rev. **145**, 1041 (1966).

7. I. Bialynicki-Birula, in *Progress in Optics*, Ed. E. Wolf (Elsevier, Amsterdam, 1996), Vol. 36.

8. W. P. Grice and I. A. Walmsley, Phys. Rev. A **56**, 1627 (1997).

9. C. K. Law, I. A. Walmsley, and J. H. Eberly, Phys. Rev. Lett. **84**, 5304 (2000), and references within.

10. H. Huang and J. H. Eberly, J. Mod. Opt. **40**, 915 (1993).

11. W. P. Grice, A. B. U'Ren, and I. A. Walmsley, Phys. Rev. A **64**, 063815 (2001).

12. T. E. Keller and M. H. Rubin, Phys. Rev. A **56**, 1534 (1997).

13. C. K. Hong, Z. Y. Ou, and L. Mandel, Phys. Rev. Lett. **59**, 2044 (1987).

14. A. B. U'Ren, K. Banaszek, and I. A. Walmsley, Quantum Inform. Comput. **3**, 480 (2003).

15. Z. D. Walton, A. V. Sergienko, B. E. A. Saleh, and M. C. Teich, quant-ph/0405021 (2004).

16. V. Giovannetti, L. Maccone, J. H. Shapiro, and F. N. C. Wong, Phys. Rev. A **66**, 043813 (2002).

17. J. Rarity, T. Wall, K. Ridley, *et al.*, Appl. Opt. **39**, 6746 (2000).

18. A. B. U'Ren, C. Silberhorn, K. Banaszek, and I. A. Walmsley (in press).